frontiers in Nanotechnology

TYPE Original Research
PUBLISHED 24 August 2026
DOI 10.3389/fnano.2026.1900378

OPEN ACCESS

EDITED BY
Zhong Sun,
Peking University, China

REVIEWED BY
Dip Das,
University College London,
United Kingdom
Yisen Wang,
Lanzhou University, China

*CORRESPONDENCE
Davide Pilati,
davide.pilati@polito.it
Gianluca Milano,
g.milano@inrim.it
Carlo Ricciardi,
carlo.ricciardi@polito.it

RECEIVED 04 June 2026
REVISED 03 July 2026
ACCEPTED 27 July 2026
PUBLISHED 24 August 2026

CITATION
Pilati D, Michieletti F, Milano G and Ricciardi C (2026) The role of areal mass density on spatiotemporal dynamics of multiterminal memristive nanowire networks.
Front. Nanotechnol. 8:1900378.
doi: 10.3389/fnano.2026.1900378

The role of areal mass density on spatiotemporal dynamics of multiterminal memristive nanowire networks

Davide Pilati[1,2]*, Fabio Michieletti[2], Gianluca Milano[2]* and Carlo Ricciardi[1]*

[1]Department of Applied Science and Technology, Politecnico di Torino, Turin, Italy, [2]Advanced Materials Metrology and Life Sciences Division, Istituto Nazionale di Ricerca Metrologica, Turin, Italy

Self-organizing memristive nanowire networks are promising substrates for physical reservoir computing because their computational properties emerge from complex spatiotemporal dynamics distributed across the network. However, how these dynamics rely on material-level parameters set during self-assembly remains insufficiently understood. Here, we investigate the impact of nanowire (NW) areal mass density (AMD) on the spatiotemporal response and computing-related properties of multiterminal Ag-PVP NW networks. We analyze the dependence of spatiotemporal dynamics on areal mass density by combining correlation analyses, temporal network response, and the impact of local properties on computational capabilities evaluated on computational benchmarks. Results show that lower-density networks exhibit weaker global correlation, slower average dynamics, longer autocorrelation times, and a broader spatial distribution of electrodes contributing to memory capacity. In contrast, denser networks show faster and more predictable responses with reduced fading memory. These findings indicate that nanowire AMD does not simply tune the overall conductance of the network, but also controls the balance between connectivity, temporal persistence, and synchronization. AMD therefore emerges as a key experimental parameter for designing multiterminal NW networks with targeted dynamical regimes for neuromorphic and reservoir-computing applications.

KEYWORDS
memristive networks, nanowire networks, neuromorphic computing, spatiotemporal characterization, unconventional computing

1 Introduction

Self-assembled networks of nanoscale objects have emerged as promising platforms for unconventional computing because their collective electrical response can give rise to complex, bio-inspired dynamics (Caravelli et al., 2025; Milano et al., 2021; Mallinson et al., 2024; Qi et al., 2023). In this context, Ag–PVP nanowire (NW) networks are particularly attractive for physical reservoir computing, as they combine nonlinear response, adaptive conductance, and distributed spatiotemporal activity within a simple self-assembled architecture (Pilati et al., 2024; Michieletti et al., 2025; Diaz-Alvarez et al., 2019; Hochstetter et al., 2021; Kotooka et al., 2021). Their computational properties arise from the collective evolution of a huge amount of interacting memristive junctions, making the network dynamics itself central to information processing (Pilati et al., 2024; Milano et al., 2020). Within the physical reservoir computing framework, computation relies on the ability of a physical system to transform input signals into a high-dimensional dynamical state space that is then analyzed by a trained readout layer (Nakajima, 2020). These networks are fabricated bottom-up through a self-assembly process, by depositing the nanowires from a suspension onto an insulating substrate, so that network connectivity, conductivity and dynamics can be tuned by varying the deposited nanowire areal density (Sannicolo et al., 2018). For NW networks, the complex behavior is closely related to the coexistence of memory effects, nonlinearity, and spatially distributed electrical activity (Michieletti et al., 2025; Hochstetter et al., 2021; Daniels et al., 2022; Loeffler et al., 2023). In particular, this behavior is due to the memristive nature of these devices, which is well documented in literature (Milano et al., 2021). Each NW junction acts as an ECM cell, where the formation and dissolution of an Ag filament is responsible for tuning the junction conductance based on the history of the applied electrical stimulus (Milano et al., 2021). Although previous studies have demonstrated the potential of these systems for computation, establishing a clear relationship between their physical characteristics and their information-processing capabilities still remains challenging (Milano et al., 2021; Pilati et al., 2024). This is due to the large number of factors that can influence the response, including the applied bias, the conductive state of the system, environmental conditions, and the network morphology (Michieletti et al., 2025; Hochstetter et al., 2021). Among these parameters, NW areal mass density (AMD) is expected to play an important role because it directly affects the number of possible junctions and conductive pathways, and therefore the overall connectivity of the network (Pantone et al., 2018; Milano et al., 2022). However, its influence on the spatiotemporal dynamics of multiterminal NW networks is still not fully explored. In particular, conventional two-terminal measurements provide only a global description of the electrical response, whereas the internal processes relevant for computation are inherently distributed across the network (Pilati et al., 2024; Michieletti et al., 2025). A multiterminal approach is therefore needed to investigate how different regions of the system evolve in space and time under electrical stimulation (Milano et al., 2026). In this work, we investigate the impact of NW network AMD on the spatiotemporal dynamics of Ag-PVP NW networks using a 4 × 4 multiterminal electrode array (Pilati et al., 2025). We analyze networks over a range of densities by combining correlation analysis, temporal characterization, and computational benchmarks (Pilati et al., 2026). The aim is to clarify how AMD shapes the dynamical behavior of the network and how these changes relate to its computing-relevant properties in a multiterminal configuration.

2 Materials and methods

2.1 Sample fabrication

Ag-PVP NW networks were fabricated on 1 × 1 cm quartz substrates by drop-casting a commercially available suspension of Ag NWs in isopropyl alcohol (IPA), as detailed in previous works (Michieletti et al., 2025). In brief, the network AMD was controlled by diluting the initial suspension with the appropriate amount of IPA before deposition. After drop-casting, the solvent was allowed to evaporate under ambient conditions, yielding self-assembled NW networks with different AMDs. To provide a baseline electrical characterization of the fabricated samples, the pristine two-terminal conductance between electrodes 1 and 16 was measured as a function of NW density before multiterminal analysis (Figure 1).

2.2 Multiterminal characterization setup

Electrical characterization was performed using a custom multiterminal fixture consisting of 16 gold-plated spring-loaded pogo pins arranged in a 4 × 4 grid to realize a multiterminal memristive device (Figure 1a). The contact array is pressed onto the sample surface so that the mechanical force of the pins locally can disrupt the PVP shell and establish electrical contact with the Ag NW core (Pilati et al., 2025). The electrodes were connected to an ArC TWO characterization board equipped with 16 source-measurement units (SMUs), enabling simultaneous electrical stimulation and readout from all terminals (Foster et al., 2022). Details on the multiterminal characterization setup can be found in (Pilati et al., 2025).

2.3 Measurement protocol and computational analysis

For the measurements and computing benchmarks, one electrode located at a corner of the array was used as the bias input, while the opposite corner electrode was used as ground, in order to maximize the effective signal propagation across the network (Milano et al., 2021). The remaining 14 electrodes were used as floating readout nodes. During operation, the input voltage was applied through the bias electrode, current was measured at the biased and grounded terminals, and the floating voltages at the other electrodes were recorded simultaneously to probe the internal state of the network. The computational analysis was performed within a physical reservoir computing framework, where the multiterminal NW network acts as the physical reservoir (more details in Supporting Information S1). (Liang et al., 2024) The recorded floating voltages from the 14 readout electrodes were used as reservoir states for the benchmark tasks. Data processing and reservoir computing analysis were carried out in Python using the RCbench package, developed for the benchmarking of physical reservoir systems (Pilati et al., 2026). The study was conducted on 45 samples in total, with three samples analyzed for each density value in the investigated range between 11.9 and 39 mg/m^2. This procedure enabled direct comparison of the effect of density on spatiotemporal network dynamics.

3 Results

3.1 Pristine conductance

Before analyzing the multiterminal spatiotemporal response, the pristine two-terminal conductance measured between electrodes 1 and 16 was evaluated as a function of NW density. As shown in Figure 1b, the pristine conductance follows a roughly sigmoid-like dependence on density (Milano et al., 2022), with a low-conductance branch at low densities, a clear activation jump around 30 mg/m^2,

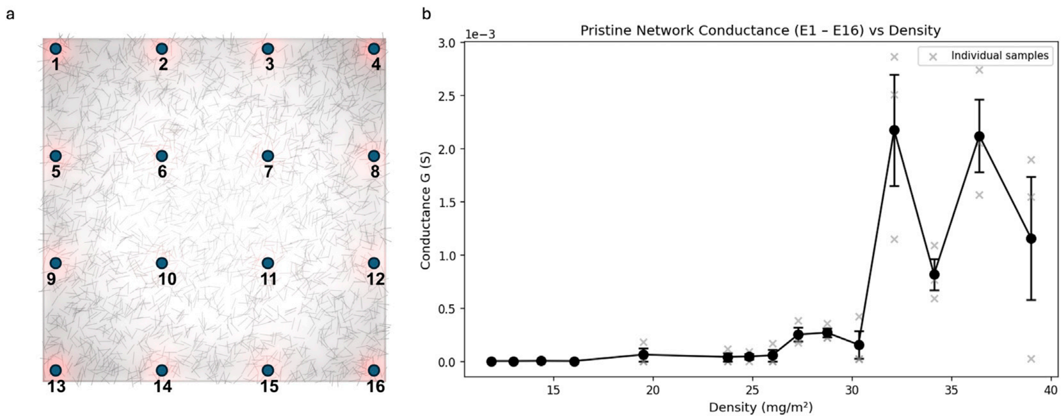

FIGURE 1
(a) Electrode disposition on a NW network sample. **(b)** pristine state conductances evaluated by imposing a reading potential (10 mV) between electrodes 1 and 16 while measuring the current.

and a high-conductance branch above the jump. This trend is well studied in network literature and specifically in memristive NW networks. The sigmoid-like dependence of pristine conductance on AMD arises from a percolation-driven transition in the Ag–PVP nanowire network, where increasing nanowire density progressively enhances interwire connectivity and junction density, producing low conductance below the percolation threshold, rapid conductance activation near the critical density, and saturation at high densities (Milano et al., 2022). Due to the discretization of the density space used for this study, the AMD threshold is derived by looking at the general behavior of the network, which shows first signs of global activation towards 25 mg/m^2 and conductance saturation above 32 mg/m^2. Sample-to-sample variability is largest across the jump. Around the activation jump, the effective large-scale connectivity between the two corner electrodes is expected not to be determined by density alone but is expected to also depend on the specific spatial arrangement of conductive pathways formed during self-assembly. In this context, it's worth mentioning that the existence of a structural backbone connecting stimulating electrodes alone does not guarantee the existence of a conductive pathway for current to flow. Indeed, a conductive pathway is present only if memristive cells along the structural pathway allow electronic conduction. Results highlight that samples with similar AMD may still exhibit different initial two-terminal conductance states between electrodes 1 and 16, motivating the need for multiterminal analysis to resolve the internal dynamical organization of the network.

3.2 Pairwise zero-lag correlation

For each pair of electrodes, the pairwise zero-lag correlation is a statistical measure of how two variables change together at the same time without any time delay. This implies the analysis of the Pearson coefficient between the two voltage signals over the recording window: a value between −1 and 1 that quantifies how synchronously the two electrodes respond. Computing this coefficient for every electrode pair yields a symmetric matrix whose structure summarizes whether the network responds in a coordinated (homogeneous) or differentiated (heterogeneous) way. Pairwise zero-lag correlation matrices were used to evaluate the similarity between signals measured at different electrodes and to assess how NW AMD affects the spatiotemporal organization of the network response. This analysis provides information on the degree of coupling between different regions of the network and on the balance between global coordination and local dynamical heterogeneity. The matrices reported in Figure 2 reveal a clear density dependence. In particular, the most heterogeneous patterns are observed below the activation jump shown in Figure 1b, at densities up to about 30 mg/m^2, where highly correlated and weakly correlated electrode pairs coexist within the same sample. This indicates a strongly differentiated response, consistent with uneven signal propagation across a sparse conductive backbone in which only a subset of pathways carries most of the current. At higher densities, above the AMD threshold, the matrices become progressively more uniform and dominated by high correlation values, reflecting a transition toward a more homogeneous and synchronized collective behavior. Overall, these results show that the sparse-connectivity regime is associated with the strongest spatiotemporal operative heterogeneity, whereas increasing density drives the network toward global coordination.

3.3 Temporal dynamics

Temporal dynamics were investigated as a function of NW density through fading-memory profiles and spectral centroid analysis (Khodakarami et al., 2025). These metrics describe the characteristic timescales of the network response and the persistence of temporal correlations in the measured signals (Hochstetter et al., 2021; Loeffler et al., 2023; Barančok and Farkaš, 2014). Analysis of fading-memory profiles and spectral centroid analysis are reported in Figures 3a,b, respectively. The fading-memory profiles in Figure 3a show that lower-density networks retain higher autocorrelation values over longer lags, with a smoother and slower decay. This corresponds to a longer persistence of past input information at low density, whereas denser

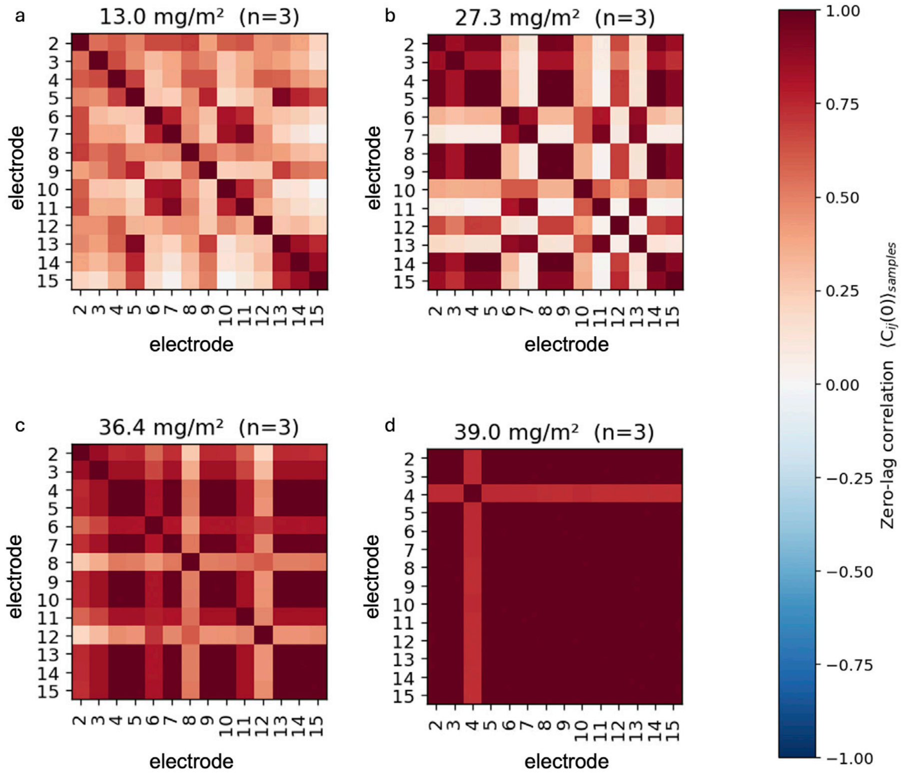

FIGURE 2
Zero-lag pairwise correlation matrices for increasing NW network densities: **(a)** 13.0 mg/m², **(b)** 27.3 mg/m², **(c)** 36.4 mg/m², and **(d)** 39.0 mg/m² averaged over three NW networks for each density value.

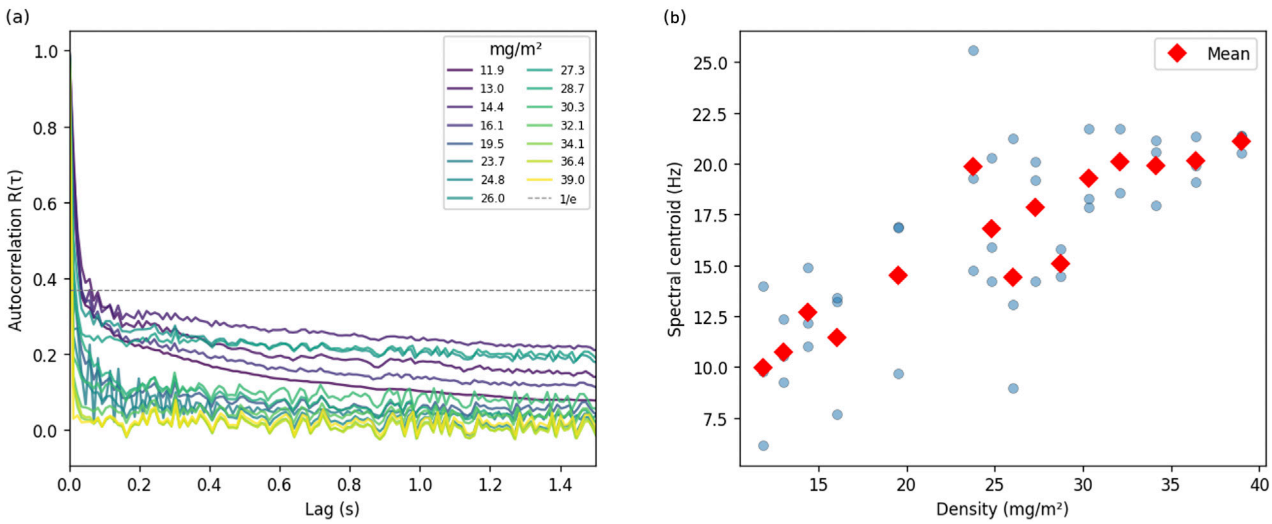

FIGURE 3
Temporal dynamics analysis as a function of NW density. **(a)** Fading memory profiles computed as autocorrelation as a function of the lag. **(b)** Mean spectral centroid as a function of density.

networks discard prior inputs more rapidly. Figure 3b reports the spectral centroid of the recorded voltage signals as a function of density. The spectral centroid is the amplitude-weighted mean frequency of the signal's power spectral density and gives a compact summary of where the spectral content sits: low values reflect a response dominated by slow, low-frequency components, while high values indicate that fast components carry most of the spectral weight. We adopt this descriptor because it captures the

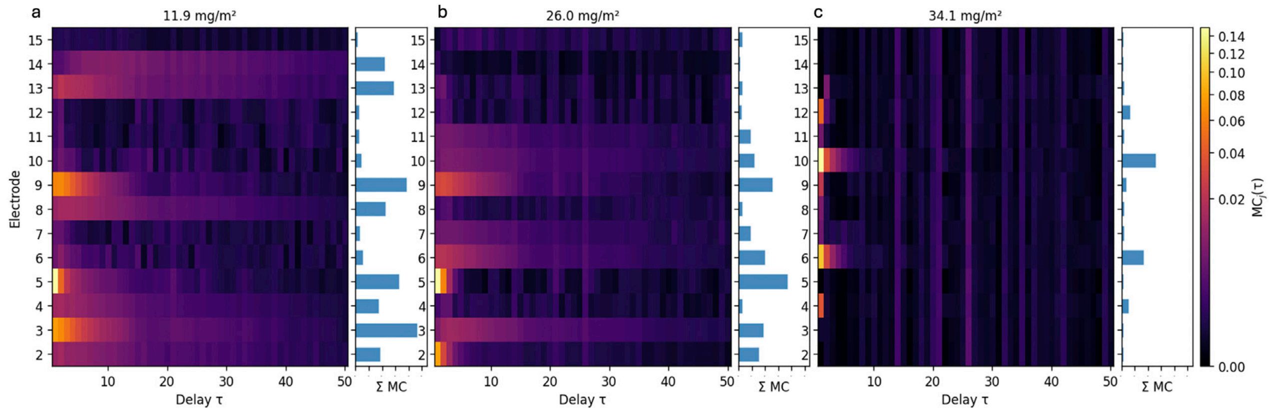

FIGURE 4
MC analysis using heatmaps depicting the single electrode contribution as a function of the delay. The analysis has been conducted on **(a)** 11.9 mg/m², **(b)** 26.0 mg/m², and **(c)** 34.1 mg/m² NW network samples. Cumulative contribution for each electrode is reported on the right side of each heatmap.

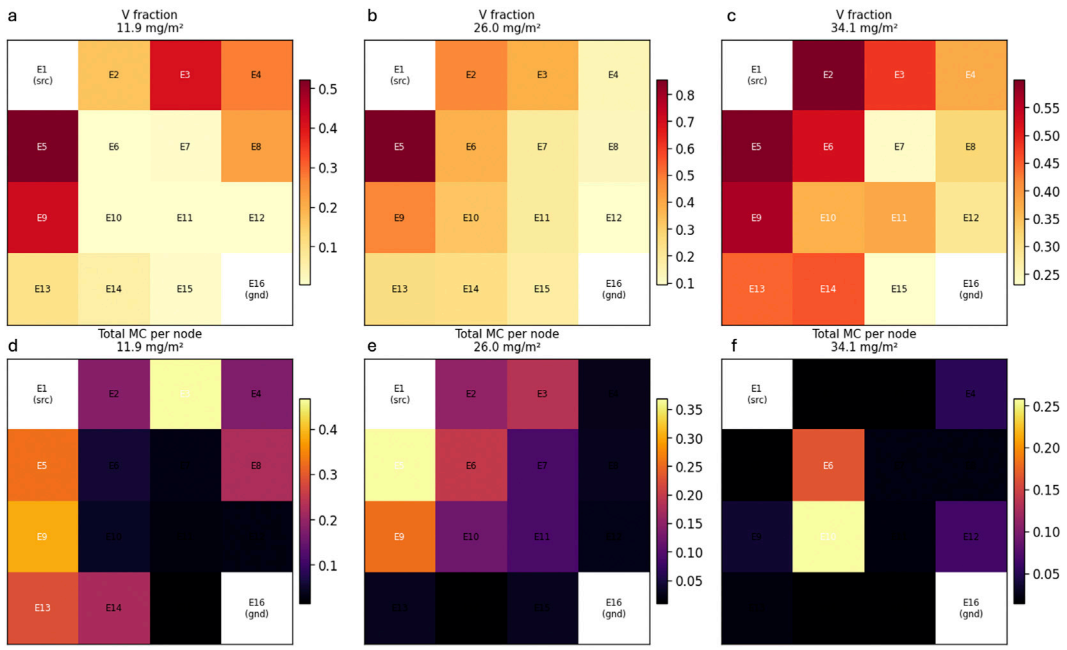

FIGURE 5
Spatial distribution of network response and memory-related electrode contributions for different nanowire densities. **(a–c)** Voltage spatial distribution heatmaps across the electrode array. **(d–f)** Heatmaps of electrode importance derived from the MC analysis. While the voltage maps provide a direct representation of the spatial response of the network, the MC heatmaps more clearly reveal the effect of density on the distribution of computationally relevant contributions across the electrodes.

characteristic response speed of the network without assuming a particular timescale model. The spectral centroid increases monotonically with density, indicating that denser networks respond on shorter timescales. This behavior is expected from network literature, where studies demonstrate how a more interconnected network has faster information flow (Cipollini and Schomaker, 2025; ACM, 2024; Ghavasieh and De Domenico, 2024). Taken together, these results show that decreasing density shifts the network toward slower temporal dynamics, while increasing density produces faster responses.

3.4 Influence of electrode response on memory capacity

The spatial distribution of memory-related features (Figures 4a–c) was investigated by evaluating the contribution of each electrode to the memory capacity (MC) benchmark task as a function of delay (Pilati et al., 2026; Wringe et al., 2025). This analysis reveals how temporal information is distributed across the multiterminal network and how this distribution changes with NW density. At low density, the MC maps show that relevant contributions are unevenly distributed across the array, with a pronounced electrode-to-electrode contrast indicative of a spatially heterogeneous representation of temporal information. At intermediate density, the overall contribution decreases and the electrode-to-electrode contrast narrows, with contributions becoming more uniform across the array. At the highest density, memory-related contributions are strongly reduced and become nearly absent across the array, resulting in a uniformly low response. The cumulative electrode contributions confirm this trend, showing a progressive reduction in both the electrode-to-electrode variability and the overall amplitude of the memory response as density increases. These results show that increasing NW density progressively suppresses and homogenizes the spatial distribution of memory-related contributions across the array, driving the network from a spatially heterogeneous to a more homogeneous regime.

3.5 Spatial dynamics

Spatial dynamics were analyzed by comparing the voltage distribution across the electrode array with the electrode importance obtained from the MC analysis, as shown in Figure 5. Figures 5a–c report snapshots of voltage maps for representative NW densities, whereas Figures 5d–f show the corresponding total MC contribution associated with each electrode. The voltage maps indicate that NW density influences the spatial distribution of the electrical response across the multiterminal network (Pilati et al., 2024). For all densities, the response is spatially nonuniform, confirming that different regions of the network contribute differently to the propagation of the input signal. For denser NW networks the response is more symmetric on the diagonal, as expected, while for sparser networks the response is more asymmetric. However, the effect of density is not immediately interpretable in computational terms from the voltage maps alone, since the observed variations do not directly identify which electrodes provide the most relevant contribution to information processing. This aspect becomes clearer in the MC heatmaps (Figures 5d–f). At lower density, memory-related contributions are distributed across multiple electrodes, indicating a broader spatial participation in the representation of temporal information. With increasing density, the MC contribution becomes progressively more localized and weaker, and at the highest density it is strongly suppressed throughout the array. Therefore, while the voltage maps show that density modifies the spatial response of the network, the MC analysis is needed to reveal how these changes affect the spatial distribution of computationally relevant activity.

4 Discussion

The present results indicate that NW AMD plays a central role in shaping the spatiotemporal response of multiterminal memristive NW networks. Taken together, the analyses show that AMD does not simply modulate connectivity strength, but more fundamentally controls the balance between local dynamical heterogeneity and global synchronization. In particular, the correlation analysis reveals that the strongest heterogeneity is observed in the sparse-connectivity regime, below the threshold AMD shown in Figure 1b, whereas the highest densities are characterized by a more uniform and coordinated response. This transition has direct implications for information processing. In the sparse-connectivity regime, the coexistence of highly correlated and weakly correlated responses of electrode pairs indicates a richer internal dynamical organization, in which different regions of the network evolve with different degrees of coupling and contribute unequally to the overall response of the network. Such spatial differentiation is consistent with the spatially heterogeneous distribution of memory-related contributions observed in the MC analysis and with the longer temporal persistence emerging from the fading-memory analysis. By contrast, increasing density progressively drives the network toward a more homogeneous response, reducing the diversity of accessible internal states and, consequently, the temporal richness available for computation. The temporal analysis supports this interpretation. Networks in the lower-density range exhibit longer fading memory and a smoother decay of past inputs, whereas denser networks respond faster, with the spectral centroid shifting toward higher frequencies. This points to a density-dependent trade-off between persistence and speed of response: lower densities favor longer temporal traces of the input, while higher densities favor faster but less memory-rich dynamics. In this sense, NW AMD can be exploited as a key experimental parameter to regulate the temporal operating regime of the network. The spatially resolved analyses further show that density affects not only the overall response, but also the way in which computationally relevant activity is distributed across the multiterminal network. The voltage maps demonstrate that the electrical response remains spatially nonuniform over the full density range, confirming that different regions of the network contribute differently to signal propagation. However, these maps alone do not directly identify the electrodes that are most relevant for computation. This becomes clearer when considering the MC electrode-importance maps, which show that lower-density networks display a spatially heterogeneous distribution of memory-related contributions across the array, with pronounced electrode-to-electrode contrast, whereas increasing density progressively suppresses these contributions and homogenizes their spatial distribution. At the highest densities, memory-related activity is strongly suppressed across the network. In conclusion, these results indicate that the most useful computational regime is not the most synchronized one, but rather a condition in which sufficient connectivity coexists with substantial spatiotemporal heterogeneity. In the present system, this condition is most evident in the sparse-connectivity regime, below the activation jump shown in Figure 1b, where the network shows the strongest spatial differentiation while still maintaining distributed signal propagation. Within this framework, NW AMD emerges as an effective design parameter for tuning memory and the spatial distribution of processing in multiterminal neuromorphic networks.

Data availability statement

The raw data supporting the conclusions of this article will be made available by the authors, without undue reservation.

Author contributions

DP: Formal Analysis, Data curation, Visualization, Writing – original draft, Writing – review and editing, Conceptualization, Investigation, Methodology. FM: Methodology, Writing – review and editing. GM: Conceptualization, Supervision, Funding acquisition, Project administration, Writing – review and editing. CR: Conceptualization, Funding acquisition, Project administration, Writing – review and editing, Supervision.

Funding

The author(s) declared that financial support was received for this work and/or its publication. Results are part of a project that has received funding from the European Research Council (ERC) under the European Union's ERC Starting Grant, grant agreement "MEMBRAIN" No. 101160604. Views and opinions expressed are however those of the authors only and do not necessarily reflect those of the European Union or the European Research Council. Neither the European Union nor the granting authority can be held responsible for them.

Acknowledgments

The authors thank Danilo Serazio (INRiM) and Alessandro Cultrera (INRiM) for the technical support on the realization of the multiterminal fixture, and Davide Cipollini for the scientific discussion.

Conflict of interest

The author(s) declared that this work was conducted in the absence of any commercial or financial relationships that could be construed as a potential conflict of interest.

Generative AI statement

The author(s) declared that generative AI was not used in the creation of this manuscript.

Any alternative text (alt text) provided alongside figures in this article has been generated by Frontiers with the support of artificial intelligence and reasonable efforts have been made to ensure accuracy, including review by the authors wherever possible. If you identify any issues, please contact us.

Publisher's note

All claims expressed in this article are solely those of the authors and do not necessarily represent those of their affiliated organizations, or those of the publisher, the editors and the reviewers. Any product that may be evaluated in this article, or claim that may be made by its manufacturer, is not guaranteed or endorsed by the publisher.

Supplementary material

The Supplementary Material for this article can be found online at: https://www.frontiersin.org/articles/10.3389/fnano.2026.1900378/full#supplementary-material

References

Barančok, P., and Farkaš, I. (2014). "Memory capacity of input-driven echo state networks at the edge of chaos," in *Artificial Neural Networks and Machine Learning ICANN* (Springer International Publishing), 41–48. doi: 10.1007/978-3-319-11179-7_6

Caravelli, F., Milano, G., Stieg, A., Ricciardi, C., Brown, S. A., and Kuncic, Z. (2025). Self-organising memristive networks as physical learning systems. doi: 10.48550/arXiv.2509.00747

Cipollini, D., and Schomaker, L. (2025). Tree networks of real-world data: analysis of efficiency and spatiotemporal scales. *Phys. Rev. Res.* 7, 033009. doi: 10.1103/ztmk-glc4

Daniels, R. K., Mallinson, J. B., Heywood, Z. E., Bones, P. J., Arnold, M. D., and Brown, S. A. (2022). Reservoir computing with 3D nanowire networks. *Neural Netw.* 154, 122–130. doi: 10.1016/j.neunet.2022.07.001

Diaz-Alvarez, A., Higuchi, R., Sanz-Leon, P., Marcus, I., Shingaya, Y., Stieg, A. Z., et al. (2019). Emergent dynamics of neuromorphic nanowire networks. *Sci. Rep.* 9, 14920. doi: 10.1038/s41598-019-51330-6

ACM (2024). Fast broadcast in highly connected networks. *Proceedings of the 36th ACM Symposium on Parallelism in Algorithms and Architectures.* Available online at: https://dl.acm.org/doi/10.1145/3626183.3659959.

Foster, P., Huang, J., Serb, A., Stathopoulos, S., Papavassiliou, C., and Prodromakis, T. (2022). An FPGA-based system for generalised electron devices testing. *Sci. Reports* 12, 13912. doi: 10.1038/s41598-022-18100-3

Ghavasieh, A., and De Domenico, M. (2024). Diversity of information pathways drives sparsity in real-world networks. *Nat. Phys.* 20, 512–519. doi: 10.1038/s41567-023-02330-x

Hochstetter, J., Zhu, R., Loeffler, A., Diaz-Alvarez, A., Nakayama, T., and Kuncic, Z. (2021). Avalanches and edge-of-chaos learning in neuromorphic nanowire networks. *Nat. Commun.* 12 (1), 1–13. doi: 10.1038/s41467-021-24260-z

Khodakarami, S., Oommen, V., Bora, A., and Karniadakis, G. E. (2025). *Mitigating Spectral Bias in Neural Operators via High-Frequency Scaling for Physical Systems.* doi: 10.48550/arXiv.2503.13695

Kotooka, T., Lilak, S., Stieg, A., Gimzewski, J., Sugiyama, N., Tanaka, Y., et al. (2021). Ag2Se Nanowire network as an effective In-Materio reservoir computing device. *ResearchSquare.* doi: 10.21203/RS.3.RS-322405/V1

Liang, X., Tang, J., Zhong, Y., Gao, B., Qian, H., and Wu, H. (2024). Physical reservoir computing with emerging electronics. *Nat. Electron.* 7, 193–206. doi: 10.1038/s41928-024-01133-z

Loeffler, A., Diaz-Alvarez, A., Zhu, R., Ganesh, N., Shine, J. M., Nakayama, T., et al. (2023). Neuromorphic learning, working memory, and metaplasticity in nanowire networks. *Sci. Adv.* 9, eadg3289. doi: 10.1126/sciadv.adg3289

Mallinson, J. B., Steel, J. K., Heywood, Z. E., Studholme, S. J., Bones, P. J., and Brown, S. A. (2024). Experimental demonstration of reservoir computing with self-assembled percolating networks of nanoparticles. *Adv. Mater.* 36, e2402319. doi: 10.1002/ADMA.202402319

Michieletti, F., Pilati, D., Milano, G., and Ricciardi, C. (2025). Self-organized criticality in neuromorphic nanowire networks with tunable and local dynamics. *Adv. Funct. Mater.* doi: 10.1002/adfm.202423903

Milano, G., Pedretti, G., Fretto, M., Boarino, L., Benfenati, F., Ielmini, D., et al. (2020). Brain inspired structural plasticity through reweighting and rewiring in multi terminal self organizing memristive nanowire networks. *Adv. Intell. Syst.* 2, 2000096. doi: 10.1002/aisy.202000096

Milano, G., Pedretti, G., Montano, K., Ricci, S., Hashemkhani, S., Boarino, L., et al. (2021). In materia reservoir computing with a fully memristive architecture based on self-organizing nanowire networks. *Nat. Mater.* 21, 195–202. doi: 10.1038/s41563-021-01099-9

Milano, G., Miranda, E., and Ricciardi, C. (2022). Connectome of memristive nanowire networks through graph theory. *Neural Netw.* 150, 137–148. doi: 10.1016/j.neunet.2022.02.022

Milano, G., Pilati, D., Michieletti, F., Cultrera, A., Ricciardi, C., and Miranda, E. (2026). Memristance and transmemristance in multiterminal memristive systems. *Sci. Rep.* 16, 5271. doi: 10.1038/s41598-026-35671-7

Nakajima, K. (2020). Physical reservoir computing—an introductory perspective. *Jpn. J. Appl. Phys.* 59, 60501. doi: 10.35848/1347-4065/ab8d4f

Pantone, R. D., Kendall, J. D., and Nino, J. C. (2018). Memristive nanowires exhibit small-world connectivity. *Neural Netw.* 106, 144–151. doi: 10.1016/j.neunet.2018.07.002

Pilati, D., Michieletti, F., Cultrera, A., Ricciardi, C., and Milano, G. (2024). Emerging spatiotemporal dynamics in multiterminal neuromorphic nanowire networks through conductance matrices and voltage maps. *Adv. Electron. Mater.* 10. doi: 10.1002/aelm.202400750

Pilati, D., Michieletti, F., Cultrera, A., Ricciardi, C., and Milano, G. (2025). "A multiterminal setup for complex dynamics characterization and unconventional computing in self-organizing memristive networks," in *2025 IEEE International Conference on Metrology for Extended Reality, Artificial Intelligence and Neural Engineering (Metroxraine)*, 1236–1241. doi: 10.1109/MetroXRAINE66377.2025.11340466

Pilati, D., Ceni, A., Michieletti, F., Gallicchio, C., Ricciardi, C., and Milano, G. (2026). RCbench: a unified framework for benchmarking reservoir computing systems. *Neuromorph. Comput. Eng.* 6, 014012. doi: 10.1088/2634-4386/ae441f

Qi, Z., Mi, L., Qian, H., Zheng, W., Guo, Y., and Chai, Y. (2023). Physical reservoir computing based on nanoscale materials and devices. *Adv. Funct. Mater.* 33. doi: 10.1002/adfm.202306149

Sannicolo, T., Charvin, N., Flandin, L., Kraus, S., Papanastasiou, D. T., Celle, C., et al. (2018). Electrical mapping of silver nanowire networks: a versatile tool for imaging network homogeneity and degradation dynamics during failure. *ACS Nano* 12, 4648–4659. doi: 10.1021/acsnano.8b01242

Wringe, C., Trefzer, M., and Stepney, S. (2025). Reservoir computing benchmarks: a tutorial review and critique. *Int. J. Parallel, Emergent Distributed Syst.*, 1–39. doi: 10.1080/17445760.2025.2472211